THE JOURNAL OF PHYSICAL CHEMISTRY C

Article

pubs.acs.org/JPCC

Theoretical Analysis on the Optoelectronic Properties of Single Crystals of Thiophene-furan-phenylene Co-Oligomers: Efficient Photoluminescence due to Molecular Bending

Hiroyuki Tamura,* Ikutaro Hamada, Hui Shang, Kazuaki Oniwa, Md. Akhtaruzzaman, Tienan Jin, Naoki Asao, Yoshinori Yamamoto, Thangavel Kanagasekaran, Hidekazu Shimotani, Susumu Ikeda, and Katsumi Tanigaki

WPI Advanced Institute for Materials Research (WPI-AIMR), Tohoku University, 2-2-1 Katahira, Aoba-ku, Sendai 980-8577, Japan

Supporting Information

ABSTRACT: We theoretically analyze the optoelectronic properties of single crystals of 2,5-bis(4-biphenylyl) bithiophene (BP2T) and 2-(4-biphenyl)-5-[5-(4-biphenyl)-2-thienyl] furan (BPFT) molecules, aiming to provide a guiding principle for the material design of organic light-emitting transistors. The X-ray structure analysis and the density functional theory (DFT) calculations indicate that half of the BPFT molecules bend the π-conjugation plane in the crystal. The Marcus theory parametrized by the DFT calculations indicates anisotropic charge mobilities. The emission spectra of the BP2T and BPFT crystals are analyzed by the time-dependent DFT calculations in conjunction with the Frenkel exciton model and the vibronic coupling analysis. We revealed that the high photoluminescence efficiency of the BPFT crystal originates from the symmetry breaking of the H-aggregate, where the transition dipole of the dark state does not cancel out.

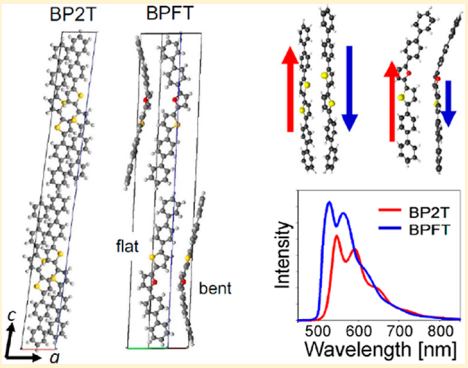

1. INTRODUCTION

Organic light-emitting transistors (OLETs)[1−13] are of great interest owing to their potential application for optoelectronic devices including electrically driven organic lasers. Organic materials have various advantages for optoelectronic devices such as the tunability of the wavelength and polarization by chemical modifications and molecular orientations. The electrically driven photoluminescence of ambipolar OLETs is realized through the injection of electron and hole from the electrodes, the charge transports in the organic layer, exciton formation, and radiative deexcitation.[1−13] While the electrically driven organic lasers have not yet been developed successfully, amplified spontaneous emissions (ASEs) have been achieved by optical pumping of organic single crystals.[7−13]

The optoelectronic properties of thiophene-based π-conjugation molecules have been investigated extensively as standard organic semiconductors for OLETs.[1−13] The single crystals of some thiophene oligomers[7,11] and thiophene-phenylene co-oligomers,[8,13,14] e.g., 2,5-bis(4-biphenylyl) bithiophene (BP2T) (Figure 1),[8,14] exhibit ASE by optical pumping.

The stacking configurations of π-conjugation molecules in organic crystals can be classified into H-aggregate and J-aggregate (Figure 2). Closely packed H-aggregates with a strong electronic coupling are generally advantageous for the charge mobility but are not favorable for the photoluminescence efficiency since in general the exciton in H-aggregates decays rapidly to the dark state.[15] The lowest exciton state of J-aggregates is optically bright, but the charge mobility along J-aggregates is generally small. That is, the trade-off between the charge mobility and the photoluminescence efficiency is a crucial problem for realizing the optoelectronic devices such as the electrically driven organic lasers.

Recently, furan-incorporated π-conjugation molecules, which can exhibit high charge mobility and efficient photoluminescence,[16,17] have attracted increasing attention as organic semiconductors for optoelectronic devices. We have recently synthesized a novel thiophene-furan-phenylene co-oligomer, namely, 2-(4-biphenyl)-5-[5-(4-biphenyl)-2- thienyl]furan (BPFT) (Figure 1),[14] aiming to improve the optoelectronic properties for OLETs. The molecular structure of BPFT is similar to BP2T except that one of the thiophene rings of BP2T is replaced with furan. It is remarkable that the BPFT crystal exhibits much higher photoluminescence efficiency[14] and ASE intensity than the BP2T crystal, while the charge mobilities of the BPFT and BP2T crystals are of the same order of magnitude.

The X-ray crystallography revealed that the BPFT crystal takes an unexpected packing structure in which half of the molecules bend the π-conjugation plane (Figure 1), while the BP2T crystal takes an ordinary herringbone packing structure. In view of the material design for OLETs, it is curious how the

Received: January 19, 2013
Revised: April 1, 2013
Published: April 4, 2013

dx.doi.org/10.1021/jp400646n | J. Phys. Chem. C 2013, 117, 8072−8078

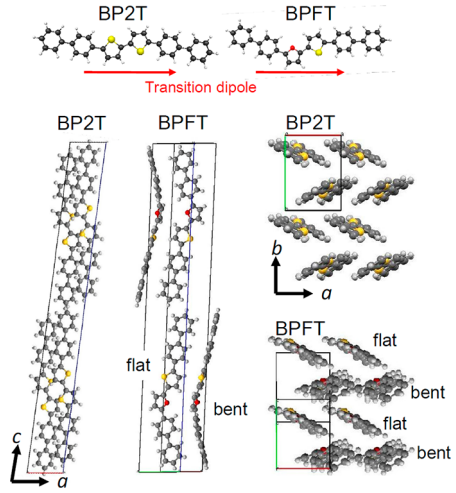

Figure 1. Molecular and crystal structures of BP2T and 2-(4-biphenyl)-5-[5-(4-biphenyl)-2-thienyl] furan (BPFT). The red arrow indicates the direction of the transition dipole of the lowest excited state. The box indicates the unit cell. The cell parameters by the X-ray structure analysis are as follows. BP2T: a = 5.71, b = 7.60, c = 52.87 (Å), α = 90.0, β = 97.1, γ = 90.0 (degree). BPFT: a = 5.79, b = 7.61, c = 49.68 (Å), α = 87.3, β = 89.2, γ = 89.9 (degree).

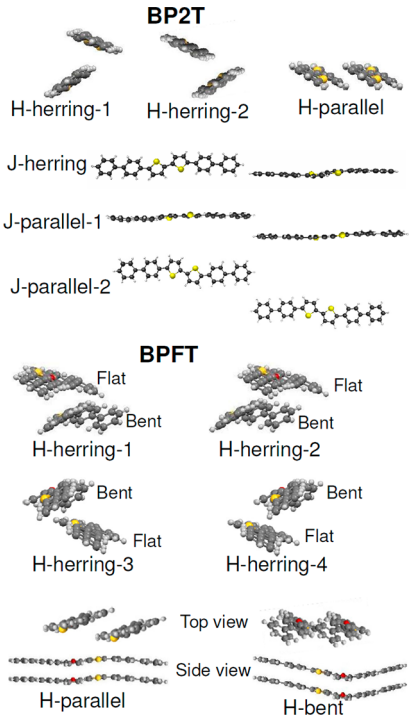

Figure 2. Configurations of H- and J-aggregates consisting of neighboring molecules in the BP2T and BPFT crystals.

bending of the π-conjugation plane in the organic crystal improves the optoelectronic properties.

In this study, we theoretically analyze the charge mobility and the photoluminescence efficiency of the BP2T and BPFT crystals, to clarify the origin of the difference in the optoelectronic properties. The angle-dependent mobilities of hole and electron are estimated by the Marcus theory parametrized by the density functional theory (DFT) calculations. The optical properties of the single crystals are analyzed based on the Frenkel exciton model and the vibronic coupling analysis parametrized by the time-dependent DFT (TDDFT) calculations. Our analysis indicates that the high photoluminescence efficiency of the BPFT crystal originates from the symmetry breaking of the H-aggregate due to the bent molecular structure.

2. THEORETICAL METHODOLOGY

2.1. Charge Mobility. The charge mobility of organic crystals can be estimated based on the Marcus theory,[18−21] when the intermolecular transfer integral is small. The intermolecular charge hopping rate by the Marcus theory reads[18]

$$W = \frac{2\pi}{\hbar}|V|^2 \frac{1}{\sqrt{4\pi\lambda k_B T}} \exp\left\{-\frac{(\Delta E - \lambda)^2}{4\lambda k_B T}\right\} \quad (1)$$

where $\hbar$ is the Plank constant; k_B is the Boltzmann constant; T is the temperature; and λ is the reorganization energy. In this study, the driving force, ΔE, is assumed to be zero. The intermolecular electronic coupling, V, reads[19−21]

$$V = \frac{J_{ij} - S_{ij}(H_{ii} + H_{jj})/2}{1 - S_{ij}^2} \quad (2)$$

where J_{ij}, S_{ij}, and H_{ii} (H_{jj}) are the transfer integral, overlap integral, and site energies, respectively.

$$J_{ij} = \langle\varphi_i|h_{ks}|\varphi_j\rangle \quad S_{ij} = \langle\varphi_i|\varphi_j\rangle$$
$$H_{ii} = \langle\varphi_i|h_{ks}|\varphi_i\rangle \quad H_{jj} = \langle\varphi_j|h_{ks}|\varphi_j\rangle \quad (3)$$

Here, φ_i is the HOMO or LUMO orbital of the single molecule relevant with the hole or electron transfer. h_{ks} is the Kohn−Sham Hamiltonian of the molecular dimer. These integrals are evaluated by the DFT with B3LYP functional, where the 6-31G(d) basis set is used. The reorganization energy is evaluated by the geometry optimization of a charged (+1 or −1) molecule. The GAMESS code[22] is used for the DFT calculations of the single molecules and the molecular aggregates. In the atomic orbital basis, φ_i and h_{ks} correspond to the vector of molecular orbital coefficients and the Fock matrix for the converged electron density, respectively.

We estimate the angle-dependent charge mobility, μ, on the $a-b$ plane of the BP2T and BPFT crystals. Here, the charge transfer along the c-axis is neglected since the BP2T and BPFT crystals take a layered structure and the interlayer electronic coupling is generally small. We define μ in the same way as in ref 21

$$\mu = \frac{e}{2k_B T}\sum_i W_i P_i R_i^2 \cos^2(\theta_i - \theta_0) \quad (4)$$

where e is the elementary charge; W_i is the charge transfer rate for the ith intermolecular hopping path; and R_i is the intermolecular center-to-center distance. P_i is the weight of the ith hopping path defined as follows

$$P_i = \frac{W_i}{\sum_i W_i} \quad (5)$$

θ_0 is the angle between the charge transport direction and the a-axis (Figure 3). θ_i is the angle between the ith hopping path and the a-axis.

2.2. Optical Property. The exciton in molecular crystals is generally described by the Frenkel exciton model.[23] Here, an

dx.doi.org/10.1021/jp400646n | J. Phys. Chem. C 2013, 117, 8072−8078

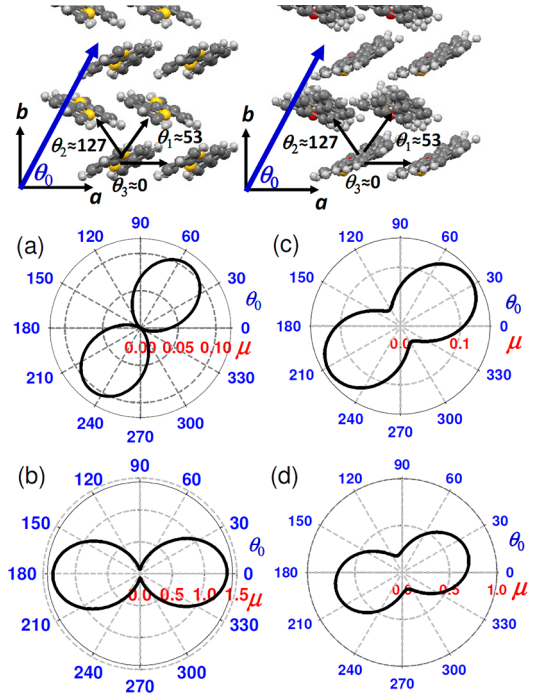

Figure 3. Calculated charge mobility, μ (radial scale: $cm^2/(V\ s)$), on the $a-b$ plane of the BP2T and BPFT crystals as a function of the charge transport angle, θ_0 (degree), with respect to the a-axis, together with the illustration of θ_0 and θ_i: (a) hole in BP2T (λ = 0.22 eV), (b) electron in BP2T (λ = 0.23 eV), (c) hole in BPFT (λ = 0.22 eV), and (d) electron in BPFT (λ = 0.22 eV), where the radius at the bold solid line indicates the charge mobility.

exciton delocalized over molecules, i.e., coherent exciton, is described by a linear combination of the excited states of single molecules as follows

$$H\Psi = E_{ex}\Psi \quad \Psi = \sum_{i=1} C_i\psi_i$$
$$H = \sum_{i=1} \varepsilon_i|i\rangle\langle i| + \sum_{i,j} h_{ij}|i\rangle\langle j| \tag{6}$$

Here, Ψ is the exciton wave function; E_{ex} is the exciton energy; and H is the Hamiltonian matrix. C_i, ψ_i, and ε_i are the amplitude, wave function, and site energy of the exciton localized at the ith molecule, respectively. h_{ij} is the intermolecular exciton coupling (off-diagonal term).

In this study, ε_i and h_{ij} are evaluated by the TDDFT calculations. The SBKJC pseudopotential[24] is used for the TDDFT calculations of the dimers, where our test calculations confirmed that the SBKJC pseudopotential predicts values of h_{ij} similar to the all-electron calculations. The TDDFT with hybrid functionals can fairly well describe the exciton states of organic materials.[25−27] We employ the long-range corrected (LC) BLYP functional[26] for the TDDFT calculations of molecular aggregates. The LC-TDDFT improves the description of charge transfer states.[26,27] When the single molecule excitation energies in the molecular aggregate are identical, i.e., $\varepsilon_1 = \varepsilon_2$ (symmetric excimer), the energy splitting of the dark and bright exciton states corresponds to the double of h_{ij} (i.e., Dayvdov splitting). When the excitation energies are not identical ($\varepsilon_1 \neq \varepsilon_2$), h_{ij} is calculated by the quasi-diabatization scheme in the same way as ref 28. In the quasi-diabatization scheme, the adiabatic exciton states of the dimer are calculated by TDDFT, and then the diabatic (single molecule) exciton states and the Hamiltonian matrix elements, ε_i and h_{ij}, are obtained as detailed in ref 28.

The transition dipole moment, d_{ex}, and the oscillator strength, f_{ex}, of a delocalized exciton are evaluated as follows (in au)

$$\vec{d}_{ex} = \langle\psi_g|\vec{r}|\Psi\rangle = \sum_i C_i\langle\psi_g|\vec{r}|\psi_i\rangle = \sum_i C_i\vec{d}_i$$
$$f_{ex} = \frac{2}{3}E_{ex}|\vec{d}_{ex}|^2 \tag{7}$$

where ψ_g is the ground state wave function; $\vec{r}$ is the dipole operator; and d_i is the transition dipole moment of the ith molecule. In general, the lower and higher excitons of the H-aggregate are optically dark and bright, respectively, where the transition dipole of the dark state cancels out as the signs of C_i are opposite. In reverse, the lower and higher excitons of the J-aggregate are bright and dark, respectively. That is, the sign of h_{ij} of H- and J-aggregates is positive and negative, respectively.

The energies and the transition dipole moments of the exciton states are calculated by diagonalizing the Hamiltonian matrix (eq 6) under three-dimensional periodic boundary conditions, where we consider 8 × 8 × 4 (256) molecules in the unit cell. The extent to which the exciton is localized in the molecular crystal is determined by the disorder of lattice that induces inhomogeneity of h_{ij}. For analyzing the optical spectra, the lattice disorder due to thermal fluctuations is taken into account based on the Monte Carlo sampling at 300 K. Here, we assume that h_{ij} depends linearly on the molecular distance, R_{ij}, as $h_{ij} = h_{eq} + \Lambda(R_{ij} - R_{eq})$, where h_{eq} and R_{eq} are the exciton coupling and the intermolecular distance at the equilibrium, respectively. R_{ij} fluctuates randomly under a harmonic potential, $V_{ij} = \kappa(R_{ij} - R_{eq})^2$. We assume appropriate parameter ranges as Λ = 0.05 eV/Å and κ = 0.3−0.4 eV/ Å^2, although there is room for future improvement of the parameters.

The light emission of organic crystals is assumed to occur after the exciton decays to the lower states. To obtain the emission spectra under thermal equilibrium, the oscillator strength is weighted by the Boltzmann factor as follows

$$\text{Intensity}\ (E_{ex}) = \frac{\exp(-E_{ex}/kT)}{Z} f_{ex}(E_{ex}) \tag{8}$$

where Z is the partition function.

The emission spectrum accounting for the vibronic coupling, i.e., the Franck−Condon factor, is calculated as follows. We calculate the dynamics of vibrational wave packet on the ground state potential starting from the equilibrium position of the excited state, where the frequency and vibronic coupling of the normal modes are evaluated by the DFT calculations with the harmonic approximation. Then, the vibronic spectrum is obtained by the Fourier transform of the autocorrelation function of wave packet dynamics.

3. RESULTS AND DISCUSSIONS

3.1. Crystal Structures. The single crystal of BP2T takes a herringbone packing structure, which has been determined by the X-ray structure analysis (Figure 1). The X-ray structure analysis of the BPFT single crystal indicates that half of the BPFT molecules bend the π-conjugation plane such that the asymmetric molecular structure can be closely packed (Figure 1). Here, the bent and flat plane BPFT molecules are

dx.doi.org/10.1021/jp400646n | J. Phys. Chem. C 2013, 117, 8072−8078

Table 1. Calculated Electronic Coupling (eV) for the Hole (V_h) and Electron (V_e) Transfers between Neighboring Molecules, Where the B3LYP Functional Is Used[a]

	BP2T			BPFT		
	V_h	V_e	R	V_h	V_e	R
H-herring-1	0.0256	0.0476	4.75	0.0347	0.0610	4.78
H-herring-2	0.0063	0.0316	4.75	0.0006	0.0173	4.78
H-herring-3	0.0256	0.0476	4.75	0.0157	0.0663	4.78
H-herring-4	0.0063	0.0316	4.75	0.0082	0.0406	4.78
H-parallel	0.0077	0.0846	5.71	0.0246	0.0650	5.79
H-parallel-bent		—		0.0231	0.0664	5.79

[a] R (Å) is the center-to-center distance.

alternatively aligned along the b-axis, i.e., the herringbone stacking direction.

We calculate the equilibrium geometry of the BPFT single crystal using the DFT calculations accounting for the van der Waals interactions (vdW-DF).[29−31] We use the vdW-DF2[31] in conjunction with the C09 exchange[32] as implemented in QUANTUM-ESPRESSO code.[33] The vdW-DF calculations confirmed that the herringbone packing consisting of bent and flat molecules is indeed a stable structure of the BPFT crystal. Coexistence of the bent and flat molecules is an interesting feature of the BPFT crystal since this originates in unique optoelectronic properties of BPFT.

3.2. Charge Mobility. The reorganization energy for the charge transfers of BP2T and BPFT is found to be ∼0.22 eV. Figure 2 shows the configurations of the H- and J-aggregates in the BP2T and BPFT crystals. There are three types of H-aggregates in the BP2T crystal, namely, H-parallel, H-herring-1, and H-herring-2 configurations (Figure 2). There are six types of H-aggregates in the BPFT crystal, namely, H-parallel-flat, H-parallel-bent, and H-herring-1 to -4 (Figure 2).

The electronic couplings for the hole and electron transfers depend sensitively on the configuration of aggregate (Table 1). As a result, the calculated charge mobility exhibits pronounced anisotropy (Figure 3). While the electron mobility tends to be high along the parallel stacking direction (a-axis), the hole mobility is high along the transverse direction, i.e., 30−60° from the a-axis. The charge mobilities of the BP2T and BPFT crystals are of the same order of magnitude. Thus, regarding the intrinsic charge mobility, the maximal performance of the BP2T and BPFT crystals is expected to be similar.

3.3. Optical Property. We calculate the excitation energy (ε_i), exciton coupling (h_{ij}), and transition dipole moment (d_i) by TDDFT; these quantities govern the optical properties of organic crystals according to eqs 6 and 7. Table 2 shows the vertical excitation energy of BP2T and BPFT single molecules at the ground state geometry ($\Delta E_{absorption}$). We also define $\Delta E_{emission}$ as the vertical excitation energy at the equilibrium geometry of the lowest excited state. The calculated excitation energy of BPFT is larger than BP2T, consistent with the experimental trend. The transition dipole moments of the BP2T and BPFT single molecules are similar; therefore, the high photoluminescence efficiency of the BPFT crystal cannot be explained by the properties of a single molecule. The $\Delta E_{absorption}$ of the bent BPFT is larger than the flat one by ∼0.053 eV, where we consider the X-ray structure and omit relaxation on the excited state. The difference in $\Delta E_{emission}$ between the bent and flat BPFT molecules is assumed to be identical to the difference in $\Delta E_{absorption}$ between the bent and flat molecules.

Figure 4 summarizes the exciton coupling, h_{ij}, and the transition dipole moment, d, of the aggregates of BP2T and BPFT. The h_{ij} of H-aggregates (a−b plane) are found to be larger than those of J-aggregates (c-axis). The h_{ij} along the herringbone stacking direction (b-axis) is somewhat larger than along the parallel stacking direction (a-axis). The BP2T crystal includes three kinds of J-aggregates, namely, the herring, parallel-1, and parallel-2 configurations as shown in Figure 2, where the nearest neighbors are considered. The BPFT crystal actually includes various types of J-aggregates; however, the

Table 2. Calculated Excitation Energy and Transition Dipole Moment of the BP2T and BPFT Single Molecules, Where the B3LYP Functional Is Used

	BP2T	BPFT flat	BPFT bent
$\Delta E_{absorption}$ [eV (nm)]	2.883 (430)	2.930 (423)	2.983 (415)
$\Delta E_{emission}$ [eV (nm)]	2.403 (516)	2.472 (501)	——
d [au]	5.33	5.04	4.92

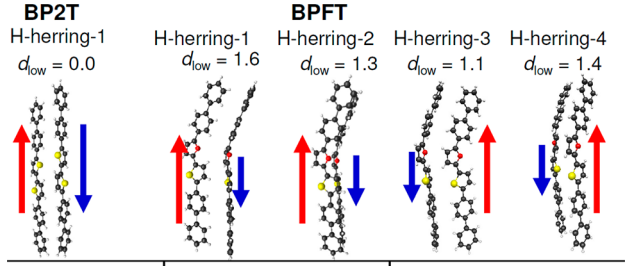

	BP2T			BPFT		
	h_{ij} (eV)	d_{low}	d_{high} (a.u.)	h_{ij} (eV)	d_{low}	d_{high} (a.u.)
H-herring-1	0.091	0.0	6.4	0.091	1.6	5.9
H-herring-2	0.091	0.0	6.4	0.095	1.3	6.0
H-herring-3	0.091	0.0	6.4	0.096	1.1	6.0
H-herring-4	0.091	0.0	6.4	0.098	1.4	6.0
H-parallel	0.070	0.0	6.4	0.069	0.0	6.1
H-bent		—		0.067	0.0	6.1
J-herring	0.019	7.0	0.0	0.018	5.5	3.7
J-parallel-1	0.020	7.0	0.3	∼0.022	∼6.7	∼0.1
J-parallel-2	0.014	6.9	0.3	∼0.012	∼6.5	∼0.6

Figure 4. Exciton coupling (h_{ij}) for the H- and J-aggregates in the BP2T and BPFT crystals, together with transition dipole moments of the lower and higher exciton states (d_{low} and d_{high}), where the LC-BLYP functional is used. Schematic illustrations of the transition dipoles of the H-aggregates are shown, where the red and blue arrows indicate the single molecule transition dipoles.

dx.doi.org/10.1021/jp400646n | J. Phys. Chem. C 2013, 117, 8072−8078

difference in h_{ij} is small among the similar configurations, and thus only representative values are shown.

While the transition dipole moment cancels out in the dark state of the BP2T H-aggregates, the transition dipole moment does not completely cancel out in the dark state of the BPFT H-aggregate consisting of the bent and flat molecules (Figure 4). In the dark state, the exciton population at the flat BPFT molecule is somewhat larger than at the bent one because of the difference in the excitation energy of the bent and flat molecules. This symmetry breaking results in a nonzero transition dipole moment of the dark state of the BPFT H-aggregate. The LC-TDDFT calculations indicate that the dark states of the H-herring-1 and H-herring-3 aggregates include ∼14% and ∼12% of charge transfer character, respectively. The charge transfer character is negligible in the exciton states of the other aggregates.

We calculate the spectra of the exciton states in the BP2T and BPFT crystals (Figure 5) based on the Frenkel exciton

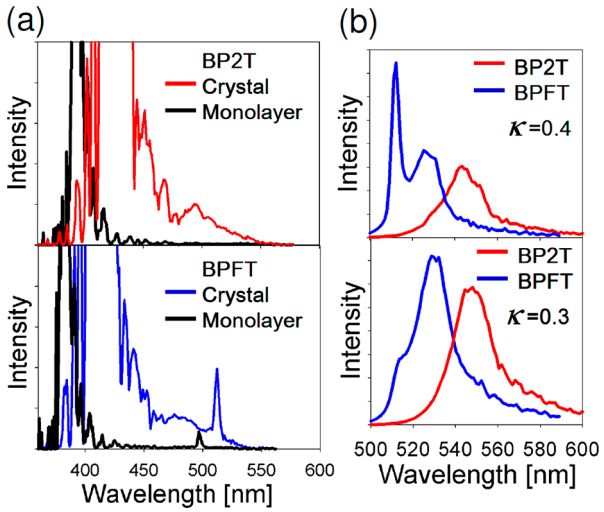

Figure 5. (a) Calculated spectra of the exciton states in the BP2T and BPFT crystals and those of the monolayers, where the scales of the BP2T and BPFT panels are identical and the fluctuation parameter, κ, is 0.4 eV/Å^2. (b) Calculated emission spectra considering the Boltzmann distribution of the exciton states at 300 K, where κ for the upper and lower panels is 0.4 and 0.3 eV/Å^2, respectively.

model parametrized by TDDFT. Here, ε_i is considered as the bottom-to-bottom excitation energy of a single molecule, and the vibronic coupling is neglected for simplicity. The long-wavelength region of the BP2T spectrum consists basically of the dark states since the exciton couplings of the H-aggregates (a−b plane) are stronger than those of the J-aggregates (c axis). The transition dipole cancels out in the dark states of the completely ordered BP2T crystal. The lattice fluctuations induce inhomogeneity of the intermolecular distances and exciton couplings, thereby increasing the net transition dipole of the dark state.

The experimental fluorescent spectra of the BP2T crystal exhibit a red-shift as compared to that of the thin film.[14] This implies that the exciton in the single crystal is more stabilized than in the thin film due to the exciton couplings along the c axis. The TDDFT calculations also predict sufficiently strong exciton couplings of J-aggregates (Figure 4), so that the exciton can be delocalized along the c axis. Indeed, the calculated spectrum of the single crystal under the periodic boundary conditions exhibits a red-shift as compared to that of the monolayer (Figure 5a).

A noticeable peak appears in the long-wavelength region of the calculated BPFT spectrum, while such a peak is not observed for BP2T (Figure 5). In this exciton state, the direction of the transition dipole is opposite at the bent and flat BPFT molecules, but the total transition dipole does not cancel out even if the lattice is completely ordered. This is because the exciton population, $|C_i|^2$, at the flat molecules tends to be larger than at the bent molecules owing to the difference in the excitation energy, ε_i. Thus, the exciton in the BPFT crystal is not quenched by the relaxation to the dark states of the H-aggregates, in contrast to the BP2T crystal that takes ordinary herringbone packing. This would be a reason why the photoluminescence efficiency of the BPFT crystal is higher than BP2T, even though the transition dipole moments of the BP2T and BPFT single molecules are similar (Table 2).

Figure 5b shows the calculated emission spectra under the assumption that the light emission occurs after the exciton decays rapidly to the lower excited states, where the Boltzmann distribution at 300 K is considered. At 300 K, the high-energy bright states are not occupied, and the emission spectrum consists of the low-energy dark states. The calculated emission intensity of the BPFT crystal is higher than that of the BP2T crystal. The peak due to the symmetry-breaking dark states of BPFT can contribute to the light emission (Figure 5b), although the peak becomes vaguer as the lattice fluctuation becomes larger.

We also analyze the influence of the vibronic coupling, i.e., the Franck−Condon factor, on the emission spectra. Figure 6a

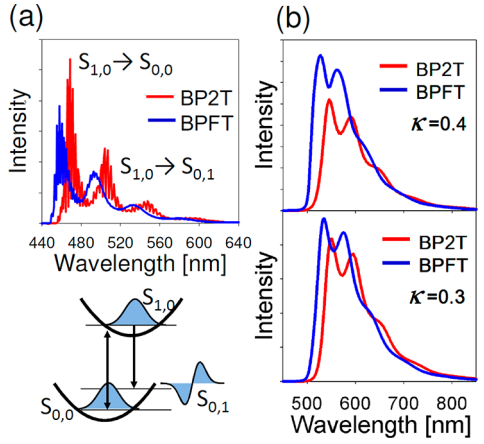

Figure 6. (a) Calculated vibronic emission spectra of the BP2T and BPFT single molecules, together with the diagram of vibronic states. (b) Calculated emission spectra of the BP2T and BPFT crystals accounting for the vibronic coupling, where the electronic spectra of the crystals (Figure 5b) are multiplied by the vibronic spectra of the single molecules (Figure 6a).

shows the vibronic emission spectra of the BP2T and BPFT single molecules calculated by the wave packet dynamics parametrized by the DFT calculations. The shortest wavelength peak corresponds to the transition from the vibrational ground state of the electronic excited state ($S_{1,0}$) to the vibrational ground state of the electronic ground state ($S_{0,0}$). The second peak corresponds to the transition from $S_{1,0}$ to the vibrational excited state of the electronic ground state ($S_{0,1}$).

The emission spectra of the BP2T and BPFT crystals (Figure 5b) are multiplied by the vibronic spectra (Figure 6a) to obtain

dx.doi.org/10.1021/jp400646n | J. Phys. Chem. C 2013, 117, 8072−8078

realistic emission spectra (Figure 6b). The emission maxima of the calculated spectra (Figure 6b) are in good agreement with those of the experimental spectra.[14] The calculated emission intensity of the BPFT crystal is higher than that of the BP2T crystal, consistent with the experimental photoluminescence efficiency. The high photoluminescence efficiency of the BPFT crystal is considered to originate from the symmetry breaking of the H-aggregates, which increases the transition dipole moments of the dark states.

4. CONCLUSION

Our theoretical analysis revealed fundamental mechanisms underlying the optoelectronic properties of the phenylene-thiophene-furan co-oligomer crystals. The asymmetric herringbone structure consisting of the bent and flat BPFT molecules originates in the remarkable optical properties. The transition dipole moment does not cancel out in the dark state of the H-aggregate consisting of the bent and flat BPFT molecules. As a result, the BPFT crystal can exhibit an efficient photoluminescence, even if the bright exciton decays rapidly to the dark states. This is contrary to the conventional picture that the exciton is quenched in closely stacked H-aggregates.

Our calculations predict anisotropic charge mobilities on the $a-b$ plane of the BP2T and BPFT crystals, where the intrinsic charge mobilities of the BP2T and BPFT crystals are comparable. The bending of π-conjugation molecules that breaks the symmetry of the H-aggregate is advantageous for increasing the charge mobility and the photoluminescence efficiency simultaneously since the exciton relaxation to the dark states does not prevent the light emission, even if the intermolecular electronic coupling is increased by decreasing the $\pi-\pi$ stacking distance. This feature provides a guiding principle for solving the trade-off between the charge mobility and the photoluminescence efficiency for OLETs.

■ ASSOCIATED CONTENT

Supporting Information

Experimental quantum yield and emission spectra of BP2T and BPFT crystals. This material is available free of charge via the Internet at http://pubs.acs.org.

■ AUTHOR INFORMATION

Corresponding Author

*Trl.: +81-80-1278-0559. E-mail: hiroyuki@wpi-aimr.tohoku.ac.jp.

Notes

The authors declare no competing financial interest.

■ ACKNOWLEDGMENTS

Advanced Institute for Materials Research (WPI-AIMR), Tohoku university, is supported by World Premier International Research Center Initiative (WPI), MEXT, Japan. H.T. is supported by the Grants-in-Aid for scientific research (C) from JSPS, Japan. I.H. is supported by a Grant-in-Aid for Scientific Research on Innovative Area "Materials Design through Computics: Complex Correlation and Non-equilibrium Dynamics" from MEXT, Japan.

■ REFERENCES

(1) Muccini, M. A Bright Future for Organic Field-Effect Transistors. *Nat. Mater.* **2006**, *5*, 605−613.
(2) Zaumseil, J.; Friend, R. H.; Sirringhaus, H. Spatial Control of the Recombination Zone in an Ambipolar Light-Emitting Organic Transistor. *Nat. Mater.* **2006**, *5*, 69−74.
(3) Takahashi, T.; Takenobu, T.; Takeya, J.; Iwasa, Y. Ambipolar Light-Emitting Transistors of a Tetracene Single Crystal. *Adv. Funct. Mater.* **2007**, *17*, 1623−1628.
(4) Takenobu, T.; Bisri, S. Z.; Takahashi, T.; Yahiro, M.; Adachi, C.; Iwasa, Y. High Current Density in Light-Emitting Transistors of Organic Single Crystals. *Phys. Rev. Lett.* **2008**, *100*, 066601−1−4.
(5) Bisri, S. Z.; Takenobu, T.; Yomogida, Y.; Shimotani, H.; Yamao, T.; Hotta, S.; Iwasa, Y. High Mobility and Luminescent Efficiency in Organic Single-Crystal Light-Emitting Transistors. *Adv. Funct. Mater.* **2009**, *19*, 1728−1735.
(6) Wang, Y.; Liu, D.; Ikeda, S.; Kumashiro, R.; Nouch, R.; Xu, Y.; Shang, H.; Ma, Y.; Tanigaki, K. Ambipolar Behavior of 2,5-Diphenyl-1,4-distyrylbenzene Based Field Effect Transistors: An Experimental and Theoretical Study. *Appl. Phys. Lett.* **2010**, *97*, 033305−1−3.
(7) Fichou, D.; Delysse, S.; Nunzi, J. First Evidence of Stimulated Emission from a Monolithic Organic Single Crystal: α-Octithiophene. *Adv. Mater.* **1997**, *9*, 1178−1181.
(8) Ichikawa, M.; Hibino, R.; Inoue, M.; Haritani, T.; Hotta, S.; Koyama, T.; Taniguchi, Y. Improved Crystal-Growth and Emission Gain-Narrowing of Thiophene/Phenylene Co-Oligomers. *Adv. Mater.* **2003**, *15*, 213−217.
(9) Ichikawa, M.; Nakamura, K.; Inoue, M.; Mishima, H.; Haritani, T.; Hibino, R.; Koyama, T.; Taniguchi, Y. Photopumped Laser Oscillation and Charge-Injected Luminescence from Organic Semiconductor Single Crystals of a Thiophene/Phenylene Co-oligomer. *Appl. Phys. Lett.* **2005**, *87*, 221113−1−3.
(10) Samuel, I. D. W.; Turnbull, G. A. Organic Semiconductor Lasers. *Chem. Rev.* **2007**, *107*, 1272−1295.
(11) Polo, M.; Camposeo, A.; Tavazzi, S.; Raimondo, L.; Spearman, P.; Papagni, A.; Cingolani, R.; Pisignano, D. Amplified Spontaneous Emission in Quaterthiophene Single Crystals. *Appl. Phys. Lett.* **2008**, *92*, 083311−1−3.
(12) Losio, P. A.; Hunziker, C.; Gunter, P. Amplified Spontaneous Emission in *para*-Sexiphenyl Bulk Single Crystals. *Appl. Phys. Lett.* **2007**, *90*, 241103−1−3.
(13) Saeki, A.; Seki, S.; Shimizu, Y.; Yamao, T.; Hotta, S. Photogeneration of Charge Carrier Correlated with Amplified Spontaneous Emission in Single Crystals of a Thiophene/Phenylene Co-oligomer. *J. Chem. Phys.* **2010**, *132*, 134509−1−7.
(14) See Supporting Information.
(15) Marciniak, H.; Fiebig, M.; Huth, M.; Schiefer, S.; Nickel, B.; Selmaier, F.; Lochbrunner, S. Ultrafast Exciton Relaxation in Microcrystalline Pentacene Films. *Phys. Rev. Lett.* **2007**, *99*, 176402−1−4.
(16) Gidron, O.; Dadvand, A.; Sheynin, Y.; Bendikov, M.; Perepichka, D. F. Towards "Green" Electronic Materials. α-Oligofurans as semiconductors. *Chem. Commun.* **2011**, *47*, 1976−1978.
(17) Mitsui, C.; Soeda, J.; Miwa, K.; Tsuji, H.; Takeya, J.; Nakamura, E. Naphtho[2,1-*b*:6,5-*b*′]difuran: A Versatile Motif Available for Solution-Processed Single-Crystal Organic Field-Effect Transistors with High Hole Mobility. *J. Am. Chem. Soc.* **2012**, *134*, 5448−5451.
(18) Marcus, R. A. Electron Transfer Reactions in Chemistry. Theory and Experiment. *Rev. Mod. Phys.* **1993**, *65*, 599−610.
(19) Senthilkumar, K.; Grozema, F. C.; Bickelhaupt, F. M.; Siebbeles, L. D. A. Charge Transport in Columnar Stacked Triphenylenes: Effects of Conformational Fluctuations on Charge Transfer Integrals and Site Energies. *J. Chem. Phys.* **2003**, *119*, 9809−9817.
(20) Deng, W.; Goddard, W. A., III Predictions of Hole Mobilities in Oligoacene Organic Semiconductors from Quantum Mechanical Calculations. *J. Phys. Chem. B* **2004**, *108*, 8614−8621.
(21) Wen, S.; Li, A.; Song, J.; Deng, W.; Han, K.; Goddard, W. A., III First-Principles Investigation of Anistropic Hole Mobilities in Organic Semiconductors. *J. Phys. Chem. B* **2009**, *113*, 8813−8819.
(22) Schmidt, M. W.; Baldridge, K. K.; Boatz, J. A.; Elbert, S. T.; Gordon, M. S.; Jensen, J. H.; Koseki, S.; Matsunaga, N.; Nguyen, K. A.;

Su, S.; et al. General Atomic and Molecular Electronic Structure System. *J. Comput. Chem.* **1993**, *14*, 1347−1363.
(23) Scholes, G. D.; Rumbles, G. Excitons in Nanoscale Systems. *Nat. Mater.* **2006**, *5*, 683−696.
(24) Stevens, W. J.; Basch, H.; Krauss, M. Compact Effective Potentials and Efficient Shared-Exponent Basis Sets for the First- and Second-Row Atoms. *J. Chem. Phys.* **1984**, *81*, 6026−6033.
(25) Igumenshchev, K. I.; Tretiak, S.; Chernyak, V. Y. Excitonic Effects in a Time-Dependent Density Functional Theory. *J. Chem. Phys.* **2007**, *127*, 114902−1−10.
(26) Towada, Y.; Tsuneda, T.; Yanagisawa, S.; Yanai, Y.; Hirao, K. A Long-Range-Corrected Time-Dependent Density Functional Theory. *J. Chem. Phys.* **2004**, *120*, 8425−8433.
(27) Körzdörfer, T.; Sears, J. S.; Sutton, C.; Brédas, J. L. Orbital Instabilities and Triplet States from Time-Dependent Density Functional Theory and Long-Range Corrected Functional. *J. Chem. Phys.* **2011**, *135*, 204107−1−4.
(28) Tamura, H.; Burghardt, I.; Tsukada, M. Exciton Dissociation at Thiophene/Fullerene Interfaces: The Electronic Structures and Quantum Dynamics. *J. Phys. Chem. C* **2011**, *115*, 10205−10210.
(29) Dion, M.; Rydberg, H.; Schröder, E.; Langreth, D. C.; Lundqvist, B. I. Van der Waals Density Functional for General Geometries. *Phys. Rev. Lett.* **2004**, *92*, 246401−1−4.
(30) Hamada, I.; Otani, M. Comparative Van der Waals Density-Functional Study of Graphene on Metal Surfaces. *Phys. Rev. B* **2010**, *82*, 153412−1−4.
(31) Lee, K.; Murray, E. D.; Kong, L.; Lundqvist, B. I.; Langreth, D. C. Higher-Accuracy Van der Waals Density Functional. *Phys. Rev. B* **2010**, *82*, 081101−1−4.
(32) Cooper, V. R. Van der Waals Density Functional: An Appropriate Exchange Functional. *Phys. Rev. B* **2010**, *81*, 161104−1−4.
(33) Giannozzi, P.; Baroni, S.; Bonini, N.; Calandra, M.; Car, R.; Cavazzoni, C.; Ceresoli, D.; Chiarotti, G. L.; Cococcioni, M.; Dabo, I.; et al. QUANTUM ESPRESSO: A Modular and Open-Source Software Project for Quantum Simulations of Materials. *J. Phys.: Condens. Matter* **2009**, *21*, 395502−1−19.